# Crystal and Molecular Structures of $[Ru(bpy)_3](PF_6)_3$ and $[Ru(bpy)_3](PF_6)_2$ at 105 K

**M. Biner,[1a] H.-B. Bürgi,*[,1b] A. Ludi,*[,1a] and C. Röhr[1b]**

*Contribution from the Institut für Anorganische Chemie, Universität Bern, CH 3000 Bern 9, Switzerland, and Laboratorium für chemische und mineralogische Kristallographie, Universität Bern, Freiestrasse 3, CH 3012 Bern, Switzerland.* *Received November 21, 1991*

**Abstract:** Dark green-black crystals of $[Ru(bpy)_3](PF_6)_3$ (III) were obtained from $[Ru(bpy)_3](PF_6)_2$ (II) by oxidation with $MnO_2$ in 7 M $H_2SO_4$. The X-ray crystal structures of III (trigonal $R\bar{3}c$, $a$ = 17.846 (7) Å, $c$ = 19.915 (7) Å, $Z$ = 6) and II (trigonal $P31c$, $a$ = 18.338 (7) Å, $c$ = 16.216 (13) Å, $Z$ = 6) were determined at 105 K. The low temperature structure of II shows the $a$- and $b$-axis increased by a factor of $\sqrt{3}$ relative to the room temperature structure and has three distinct Ru sites (phase transition at 190 (5) K). This explains many recent spectroscopic observations. The Ru-N distances of II (2.053 (2) Å) are virtually indistinguishable from those of III (2.057 (3) Å). This is compatible with the high electron self-exchange rate between II and III. The pattern of differences in intra-bpy bond lengths seems in contradiction to the conventional $\pi$-backbonding model. Changes of bpy distances in $[M(bpy)_3]$, bpy, $Hbpy^+$, and $H_2bpy^{2+}$ are examined by a principal component analysis, which yields two main factors: The first factor is related to the temperature of measurement, the crystal packing pattern or the model used to interpret the diffraction data. The second factor can be characterized as electronic in nature and confirms that there are as yet unresolved contradictions in the model of $\pi$-backbonding as applied to the ligand geometry of $[M(bpy)_3]^{n+}$ complexes.

## Introduction

Tris(bipyridine)ruthenium(II), $Ru(bpy)_3^{2+}$, has evolved from a quite esoteric complex ion of a rare platinum metal into an immensely popular, almost magic compound. Together with its numerous derivatives it has probably initiated more scientific publications than any other inorganic compound. The starting point for this impressive "research career" is its potential as an agent for solar energy conversion. Subsequent research has led to a collection of intriguing photophysical and photochemical properties of $Ru(bpy)_3^{2+}$. The vast literature has been collected and reviewed in several monographs.[2-7]

Particular attention has been devoted to the excited state, $*Ru(bpy)_3^{2+}$. The intense absorption at 454 nm is attributed to a $t_{2g} \rightarrow \pi^*$ MLCT process. The excited triplet state $*Ru(bpy)_3^{2+}$ readily reacts with an acceptor producing ground state $Ru(bpy)_3^{3+}$. Owing to its very positive reduction potential of 1.26 V this species can oxidize $OH^-$ leading to subsequent production of $O_2$. Consequently the thermodynamic as well as the kinetic aspects of this and related redox reactions have attracted considerable attention.[3,11]

Sophisticated spectroscopic techniques have been employed to address the issue whether the transferred charge is localized on one single ligand or distributed equally over all three bipyridine molecules. Careful and detailed spectroscopic studies dealing with the ground state electronic structure have been performed as well. A recent study considered the occurrence of different ruthenium sites in the trigonal lattice of $[Ru(bpy)_3](PF_6)_2$.[9] The redetermination of the crystal structure of $Ru(bpy)_3^{2+}$ at 105 K was undertaken to provide information relevant to the high resolution optical spectroscopy usually carried out at very low temperatures (<15 K).

Among the known $ML^{3+/2+}$ redox couples of ruthenium $Ru(bpy)_3^{3+/2+}$ shows the highest self-exchange rate, $k = 4.2 \times 10^8$ $M^{-1}$ $s^{-1}$.[10,11] From a comparison with the electron exchange rate of analogous iron polypyridine complexes it was concluded that $Ru(bpy)_3^{n+}$ has virtually identical coordination geometries in the oxidation states II and III. Although the orange solution of $Ru(bpy)_3^{2+}$ can be oxidized to the dark green $Ru(bpy)_3^{3+}$ by a variety of oxidants, the solid ruthenium(III) products decompose very rapidly. No crystalline product, suitable for a crystallographic study has yet been reported in the literature. In contrast to the vastly documented solid state properties for $Ru(bpy)_3^{2+}$ there is thus a surprising lack of corresponding data for the oxidized Ru(III) complex. Obviously, the molecular structure of $Ru(bpy)_3^{3+}$ has been a significant missing link in the ruthenium tris(bipyridine) saga.

This paper reports a synthesis, crystal growth, and crystal and molecular structure of $[Ru(bpy)_3](PF_6)_3$ at 105 K, a redetermination of the structure for $[Ru(bpy)_3](PF_6)_2$ at the same temperature, and the results of a principal component analysis of the intraligand distances of $[M(bpy)_3]$ complexes, bpy, $Hbpy^+$, and $H_2bpy^{2+}$.

## Experimental Section

**A. Preparation and Crystal Growth. $[Ru(bpy)_3](PF_6)_2$ (II).** Synthesis of II from the starting material $RuCl_3 \cdot xH_2O$ (Johnson Matthey) and 2,2'-bipyridine (Fluka) followed published procedures.[2,4] The microcrystalline $PF_6^-$ salt was dissolved in acetone and placed in a desiccator over diethyl ether. Orange prismatic crystals could be isolated after 2 days. Anal. Calcd. for $RuC_{30}H_{24}N_6P_2F_{12}$: C, 41.9; H, 2.8; N, 9.8; P, 7.2; F, 26.5. Found: C, 42.2; H, 2.8; N, 10.0; P, 6.6; F, 26.5.

**$[Ru(bpy)_3](PF_6)_3$ (III).** A variety of oxidants have been used to produce $Ru(bpy)_3^{3+}$.[3] Our screening experiments gave the best results with $MnO_2$: 120 mg of $[Ru(bpy)_3]SO_4 \cdot 7H_2O$ were dissolved under stirring in 3 mL of 7 M $H_2SO_4$, taking about 2 h. Addition of 18 mg of $MnO_2$ immediately produced a color change from orange to green. After 1 h excess $MnO_2$ was separated by centrifugation. One-half of this solution was transferred into a test tube and carefully covered with 1.1 mL of 0.34 M $KPF_6$. (The other half was similarly covered with 0.5 M $HPF_6$ yielding only microcrystalline product). Slow mixing of the two layers by diffusion at −20 °C afforded visibly black prismatic crystals within 4 days. Anal. Calcd. for $RuC_{30}H_{24}N_6P_3F_{18}$: C, 35.9; H, 2.4; N, 8.4; F, 34.0. Found: C, 34.0; H, 2.2; N, 8.0; F, 33.9.

**B. Data Collection.** Data were collected at 105 K on an Enraf-Nonius CAD4 automatic four-circle diffractometer with graphite monochromated Mo K$\alpha$ radiation and a low-temperature attachment.

(1) (a) Institut für Anorganische Chemie, Universität Bern. (b) Laboratorium für Kristallographie, Universität Bern.

(2) Seddon, E. A.; Seddon, K. R. *The Chemistry of Ruthenium*; Elsevier: Amsterdam, 1984.

(3) Schröder, M.; Stephenson, T. A. In *Comprehensive Coordination Chemistry*; Wilkinson, G.; Ed.; Pergamon: Oxford, England, 1987; Volume 4.

(4) Krause, R. *Struct. Bonding* **1987**, *67*, 1.

(5) Juris, A.; Balzani, V.; Barigelletti, F.; Campagna, S.; Belser, P.; Von Zelewsky, A. *Coord. Chem. Rev.* **1988**, *84*, 85.

(6) Krausz, E.; Ferguson, J. *Prog. Inorg. Chem.* **1989**, *37*, 293.

(7) Constable, E. C. *Adv. Inorg. Chem.* **1989**, *34*, 1.

(8) Rillema, D. P.; Jones, D. S.; Levy, H. A. *J. Chem. Soc., Chem. Commun.* **1979**, 849.

(9) (a) Yersin, H.; Braun, D.; Hensler, G.; Gallhuber, E. In *Vibronic Processes in Inorganic Chemistry*; Flint, C. D., Ed.; Kluwer Academic Publishers: 1989; p 195. (b) Ferguson, J.; Herren, F.; McLaughlin, G. M. *Chem. Phys. Lett.* **1982**, *89*, 376. (c) Braun, D.; Hensler, G.; Gallhuber, E.; Yersin, H. *J. Phys. Chem.* **1991**, *95*, 1067.

(10) Young, R. C.; Keene, F. R.; Meyer, T. J. *J. Am. Chem. Soc.* **1977**, *99*, 2468.

(11) Meyer, T. J.; Taube, H. In *Comprehensive Coordination Chemistry*; Wilkinson, G., Ed.; Pergamon: Oxford, England, 1987; Vol. 1, p 331.

0002-7863/92/1514-5197$03.00/0 

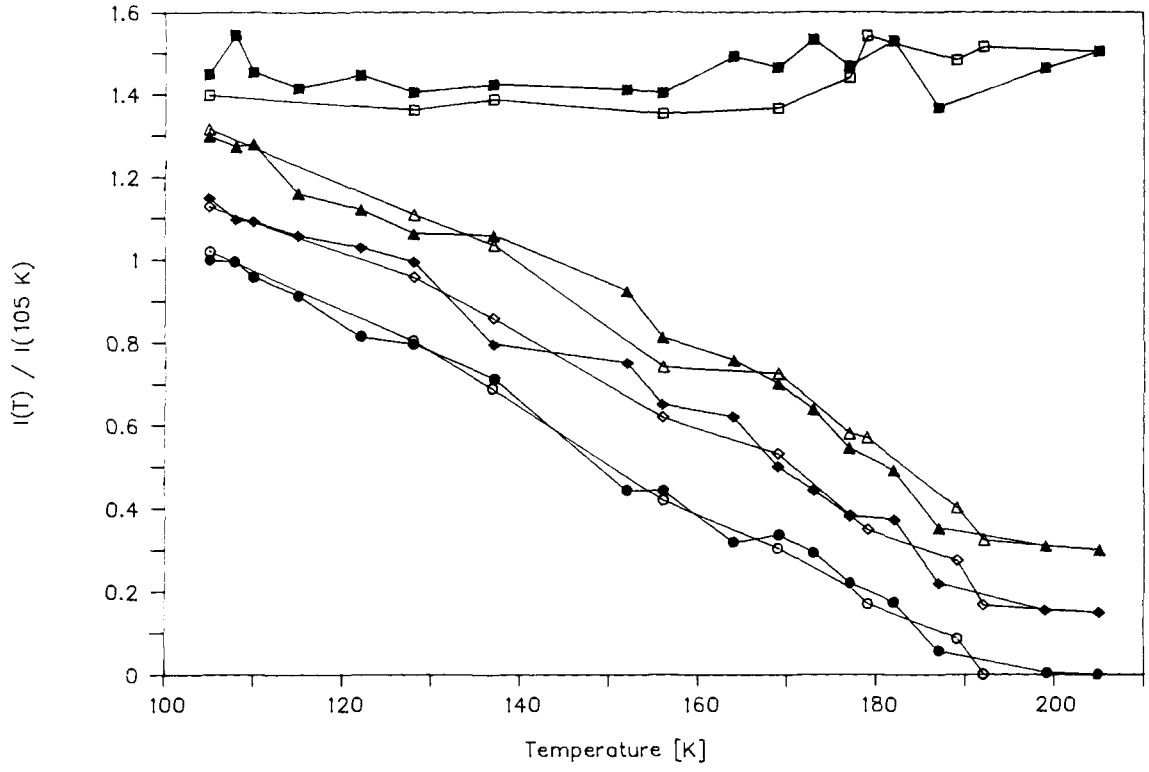


**Figure 1.** Temperature dependence of the normalized intensities of one main and three superstructure reflections during heating (filled symbols) and cooling (empty symbols). For clarity three of the four curves are shown shifted vertically ("symbol (*hkl*), shift" are given): ■, □ (−8 7 2), 0.45; ▲, △ (2 3 3), 0.3; ◆, ◇ (0 5 6), 0.15; ●, ○ (3 4 −7), 0.

**$[Ru(bpy)_3](PF_6)_3$ (III).** A black crystal of III with approximate dimensions of 0.1 × 0.1 × 0.3 mm³ mounted on the end of a quartz fiber was placed on the diffractometer. Lattice dimensions were determined by a least squares fit to the setting parameters of 23 centered reflections at room temperature. The temperature was lowered to 105 K in steps of approximately 40 K. The cell parameters were refined after each step. Data collection parameters are given as supplementary material. For crystal data see Table I.

**$[Ru(bpy)_3](PF_6)_2$ (II).** The unit cell constants of a hexagonal-prismatic shaped orange crystal of II (0.1 × 0.1 × 0.5 mm³) were calculated from the setting angles of 24 high angle reflections by a least squares procedure at 105 K. The unit cell distance $a$ was found to be larger by $\sim\sqrt{3}$ than that at room temperature. After completion of the data collection, the temperature was therefore raised from 105 K in steps of 10–20 K, and the intensities of 21 reflections were monitored as a function of $T$. Intensities of reflections with $(h - k)$ (mod 3) $\neq 0$ drop continuously with increasing temperature and reach zero at ~190 K. The slope $dI(T)/dT$ decreases slightly and reaches a minimum at ~190 K. The loss of intensity for the reflections $(h - k)$(mod 3) = 0 was not more than 60% in the same temperature range. This behavior is illustrated for both classes of reflections in Figure 1. Subsequent cooling shows that the intensity changes are reversible. Thus, at 190 K a reversible single crystal to single crystal phase transition occurs.

**C. Solution and Refinement of the Structures.** Data reduction including Lorentz, polarization, and decomposition corrections was carried out using the Enraf-Nonius Structure Determination Package.[14] A $\psi$-scan absorption correction was applied to II but not to III.

**$[Ru(bpy)_3](PF_6)_3$ (III).** Unit cell constants, X-ray powder patterns, and possible space groups suggest that III is isostructural to the corresponding Rh(III) and Cr(III) compounds.[12,13] Initial atomic coordinates taken from the Cr compound were refined using full-matrix least squares methods[15] with anisotropic displacement parameters for non-H atoms. H atoms were placed in calculated positions (C–H: 0.95 Å). The largest feature in a final difference map was 1.39 e/Å³ in the vicinity of the Ru atom.

**$[Ru(bpy)_3](PF_6)_2$ (II).** The three ruthenium atoms were located by using standard Patterson methods in space group $P31c$. The other non-H atoms were located from successive difference Fourier syntheses and refined by full-matrix least squares (SHELX76[15]). The low temperature modification ($\alpha$-II) differs little from the room temperature one ($\beta$-II). This led to high correlation among the positional parameters of corresponding atoms in the three crystallographically independent complex ions. Furthermore the intensity of the superstructure reflections $(h - k)$(mod 3) $\neq 0$ is generally low, leading to a poor ratio of parameters to observations. The refinement was therefore restrained by requiring that chemically equivalent bond distances be of equal but adjustable length to within 0.001 Å (weight for restraint conditions $(0.001)^{-2}$). The final cycles of full-matrix least squares refinement with anisotropic temperature factors for all non-H atoms, calculated H atom positions (C–H: 0.95 Å), and one isotropic hydrogen thermal parameter for all H atoms converged smoothly. The weighting scheme employed was $w = k/[\sigma^2(F) + |g|F^2]$, where both $k$ and $g$ were refined. The highest peak in the final

**Table I.** Crystallographic Data for $[Ru(bpy)_3](PF_6)_3$ and $[Ru(bpy)_3](PF_6)_2$

| | | $[Ru(bpy)_3](PF_6)_3$ | $[Ru(bpy)_3](PF_6)_2$ |
|---|---|---|---|
| chem formula | | $RuP_3F_{18}N_6C_{30}H_{24}$ | $RuP_2F_{12}N_6C_{30}H_{24}$ |
| mol wt | [g/mol] | 1004.54 | 859.57 |
| crystal dimensions | [mm³] | 0.1 × 0.1 × 0.3 | 0.1 × 0.1 × 0.5 |
| $T$ | [K] | 105 | 105 |
| cell parameters | | | |
| $a$ | [Å] | 17.846 (7) | 18.338 (7) |
| $c$ | [Å] | 19.915 (7) | 16.216 (13) |
| $V$ | [Å³] | 5493 (3) | 4722 (4) |
| space group | | $R\bar{3}c$, no. 167 | $P31c$, no. 159 |
| $Z$ | | 6 | 6 |
| $k$ | | 0.9319 | 0.7120 |
| $g$ (weight) | | 0.00254 | 0.00088 |
| no. of independent refl | | 1106 | 2540 |
| $d_{x\text{-ray}}$ at 105 K | [g/cm³] | 1.823 | 1.813 |
| $d_{obs}$ at 295 K | [g/cm³] | 1.80 | |
| $\mu$ | [cm⁻¹] | 5.98 | 6.16 |
| $R(F_o)$ | | 0.046 | 0.027 |
| $R_g$ | | 0.057 | 0.036 |

(12) Goodwin, K. V.; Pennington, W. T.; Petersen, J. D. *Inorg. Chem.* **1989**, *28*, 2016.
(13) Hauser, A.; Mäder, M.; Robinson, W. T.; Murugesan, R.; Ferguson, J. *Inorg. Chem.* **1987**, *26*, 1331.
(14) Frenz, B. A. *Structure Determination Package*; Enraf Nonius: Delft, The Netherlands, 1983.
(15) Sheldrick, G. M. SHELX76, Program for Crystal Structure Determination; University of Cambridge: England, 1976.

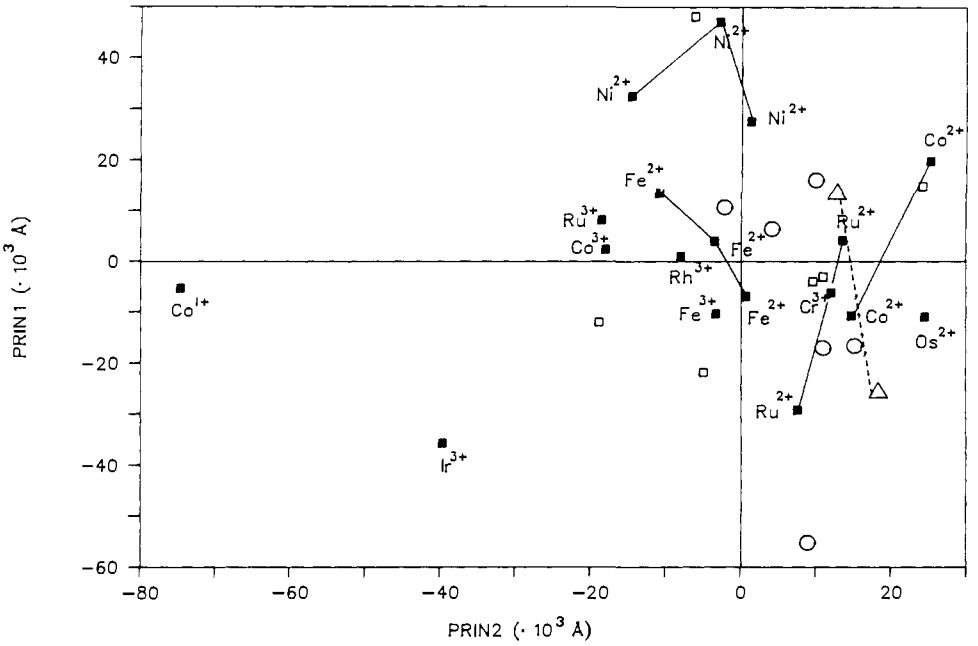


**Figure 2.** Distribution of data points in the principal component coordinate system PRIN1 vs PRIN2: (■) $[M(bpy)_3]$, (△) bpy, (○) $Hbpy^+$, (□) $H_2bpy^{2+}$.

difference Fourier map was found to be 0.37 e/Å$^3$. Determination of the polarity of the 3-fold axis is inconclusive, because the arrangement of the strongest anomalous scatterer, Ru, is close to centrosymmetric.

Final non-hydrogen atom coordinates, H atom coordinates, anisotropic thermal parameters, and observed and calculated structure factor amplitudes have been deposited as supplementary material.

**D. Principal Component Analysis of Intraligand Distances.** A systematic analysis of bond distances in the bpy ligands was carried out by principal component analysis[17,18] with the use of procedure PRINCOMP of the SAS Program Package.[19] Structural data of $[M(bpy)_3]$ complexes and free bpy, $Hbpy^+$, and $H_2bpy^{2+}$ were retrieved from the Cambridge Crystallographic Data Base (CDB),[20] if the *R* value was lower than 0.10 and if the atomic number of the heaviest element in the compound was lower than 78 (Pt). Structures with disorder in the complex cation or bpy, with Jahn–Teller distorted ions or with a wrong space group were rejected. Thirty-two data sets survived: 2 bpy,[21,22] 7 $Hbpy^+$,[23,28] 5 $H_2bpy^{2+}$,[23,24,29-31] and 18 $[M(bpy)_3]$[8,12,25,32-42] structures. The intra-bpy bond distances were averaged in each case with respect to $D_3$ ($[M(bpy)_3]$), $C_2$ (bpy, $Hbpy^+$), or $C_i$ ($Hbpy^+$, $H_2bpy^{2+}$) symmetry, producing seven variables per data set.

In a principal component analysis each type of observation, here each of the seven bond distances, is first averaged. Then the variance–covariance matrix is calculated with the deviations from mean values, and its eigenvalues and eigenvectors are obtained. An eigenvector associated with a large eigenvalue implies a direction in bond distance space in

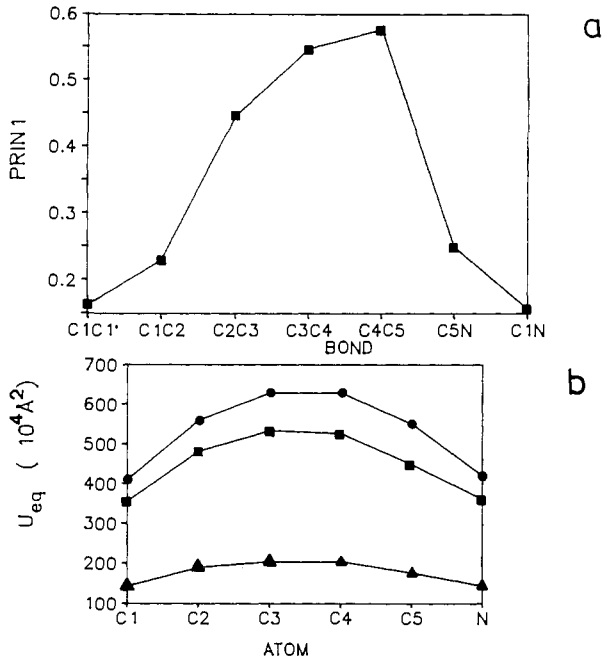


**Figure 3.** (a) Coefficients of eigenvector PRIN1 and (b) $U_{eq}$ for selected data sets: (●) $[Cr(bpy)_3](PF_6)_3$, 295 K,[12] (■) $[Fe(bpy)_3]_2Cl_2$(d-tart)·11$H_2O$, 295 K,[39] (▲) $[Ru(bpy)_3](PF_6)_3$, 105 K (this work).

(16) *International Tables of X-ray Crystallography*; Kynoch Press: Birmingham, England, 1974; Vol. IV. Tables 2.2.B, 2.2.C, 2.3.1.
(17) Murray-Rust, P.; Motherwell, S. *Acta Crystallogr.* **1978**, *B34*, 2518.
(18) Murray-Rust, P.; Motherwell, S. *Acta Crystallogr.* **1978**, *B34*, 2527.
(19) SAS Institute Inc.: SAS User's Guide Version 5 Edition; SAS Institute Inc.: Cary, NC, 1985.
(20) Allen, F. H.; Bellard, S.; Brice, M. D.; Cartwright, B. A.; Doubleday, A.; Higgs, H.; Hummelink, T.; Hummelink-Peters, B. G.; Kennard, O.; Motherwell, W. D. S.; Rodgers, J. R.; Watson, D. G. *Acta Crystallogr.* **1979**, *B35*, 2331.
(21) Chisholm, M. H.; Huffman, J. C.; Rothwell, I. P.; Bradley, P. G.; Kress, N.; Woodruff, W. H. *J. Am. Chem. Soc.* **1981**, *103*, 4945.
(22) Castro, R.; Duran, M. L.; Garcia-Vazquez, J. A.; Romero, J.; Sousa, A.; Castineiras, A.; Hiller, W.; Strähle, J. *J. Chem. Soc., Dalton Trans.* **1990**, 531.
(23) Chantler, C. T.; Maslen, E. N. *Acta Crystallogr.* **1989**, *B45*, 290.
(24) Fuller, D. J.; Kepert, D. L.; Skelton, B. W.; White, A. H. *Aust. J. Chem.* **1987**, *40*, 2097.
(25) Figgis, B. N.; Skelton, B. W.; White, A. H. *Aust. J. Chem.* **1978**, 31, 57.
(26) Parlow, A.; Hartl, H. *Z. Naturforsch.* **1985**, *B40*, 45.
(27) Lipkowski, J.; Sgarabotto, P.; Andreetti, G. D. *Cryst. Struct. Commun.* **1976**, *5*, 931.
(28) Szentivanyi, H.; Stomberg, R. *Acta Chem. Scan.* **1984**, *A38*, 101.
(29) Lipka, A. *Z. Naturforsch.* **1983**, *B38*, 1615.
(30) Preut, H.; Huber, F.; Alonzo, G. *Acta Crystallogr.* **1987**, *C43*, 46.
(31) Belin, C.; Roziere, J.; Potier, J. *Acta Crystallogr.* **1981**, *B37*, 1306.
(32) Szalda, D. J.; Creutz, C.; Mahajan, D.; Sutin, N. *Inorg. Chem.* **1983**, *22*, 2372.
(33) Yanagi, K.; Ohashi, Y.; Sasada, Y.; Kaizu, Y.; Kobayashi, H. *Bull. Chem. Soc. Jpn.* **1981**, *54*, 118.
(34) Wada, A.; Katayama, C.; Tanaka, J. *Acta Crystallogr.* **1976**, *B32*, 3194.
(35) Wada, A.; Sakabe, N.; Tanaka, J. *Acta Crystallogr.* **1976**, *B32*, 1121.
(36) Potvin, C.; Manoli, J.-M.; Sécheresse, F. *Inorg. Chim. Acta* **1990**, *168*, 173.
(37) Weiss, H.; Strähle, J. *Z. Naturforsch.* **1984**, *B39*, 1453.
(38) Garcia Posse, M. E.; Juri, M. A.; Aymonino, P. J.; Piro, O. E.; Negri, H. A.; Castellano, E. E. *Inorg. Chem.* **1984**, *23*, 948.
(39) Tada, T. *J. Sci. Hiroshima Univ.* **1982**, *A46*, 73.
(40) Hazell, A. C.; Grønbaek Hazell, R. *Acta Crystallogr.* **1984**, *C40*, 806.
(41) Huebsch, B.; Mahieu, B.; Meinier-Piret, J. *Bull. Soc. Chim. Belg.* **1985**, *94*, 685.
(42) Constable, E. C.; Raithby, P. R.; Smit, D. N. *Polyhedron* **1989**, *8*, 367.

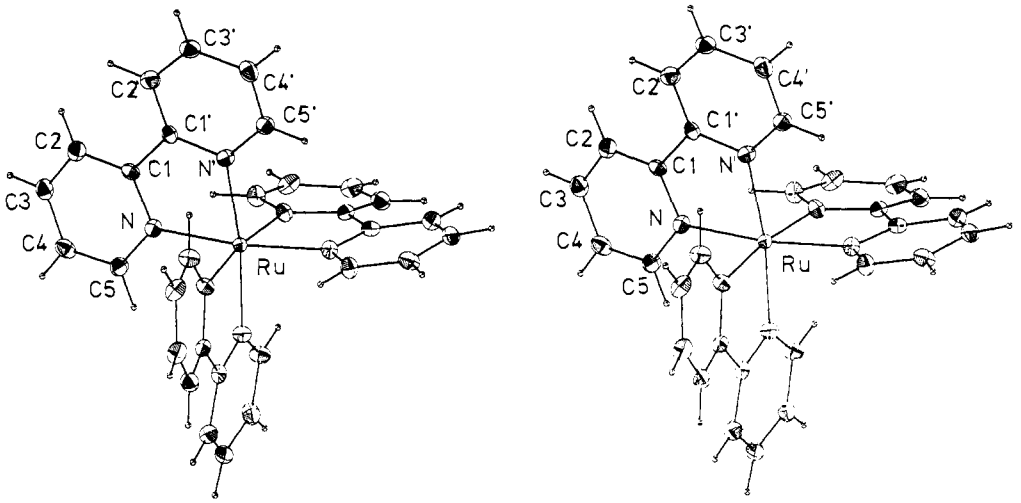


**Figure 4.** Molecular conformation of $[Ru(bpy)_3]^{3+}$ with the atom-labeling system used in the tables.

which the data points show generally large scatter from the respective mean. The eigenvectors are given as normalized linear combinations of the original variables (deviations of bond distances from their mean). The data points may then be transformed to the new coordinate system defined by the eigenvectors.

Here, the principal component analysis yields two main factors: The first (PRIN1), explaining 37% of the total variance with an eigenvalue of $4.93 \times 10^{-4}$ Å$^2$, depends on the crystal packing, the temperature of measurement, and the model used to interpret the diffraction data. It is discussed below. The second component (PRIN2, 30% of variance, eigenvalue $3.97 \times 10^{-4}$ Å$^2$) is related to the electronic structure of the complex and will be discussed in the Discussion section. The two main features are robust with respect to elimination of up to five data sets, namely outlayers like the $Co^+$, $Ir^{3+}$, and the $Ni^{2+}$ compounds (Figure 2). An analysis with only the metal complex data sets yields similar principal components except that PRIN1 now accounts for 33% of the total variance, whereas PRIN2 accounts for 43%. The remaining five components with eigenvalues between $1.54 \times 10^{-4}$ Å$^2$ and $0.30 \times 10^{-4}$ Å$^2$, corresponding to rms deviations from mean distances of 0.013–0.006 Å, are in the range of the mean standard deviation of C–C and C–N bonds (0.011 Å, as far as esd's have been published). They are not interpreted here. Figure 2 shows the distribution of data points in the PRIN1 vs PRIN2 coordinate system.

**Principal Component 1.** The coefficients defining the eigenvector belonging to PRIN1 are visualized in Figure 3a, which shows positive correlations between all seven bond distances. A large positive (negative) coordinate along PRIN1 (e.g., $Ni^{2+}$ and $Ir^{3+}$ complexes, respectively; see Figure 2) implies that distances C3C4 and C4C5 are substantially bigger (smaller) than corresponding mean values, whereas nothing can be said about the distances C1C1′ and C1N. An interpretation of PRIN1 may be based on the following observations: the two structure determinations of $[Ru(bpy)_3]^{2+}$ at 295 and 105 K show approximately the same coordinates along PRIN2, but differ in PRIN1, the room temperature structure has PRIN1 = −0.029 Å, the 105 K structure has PRIN1 = 0.004 Å. Similar behavior is observed for the two points representing bpy structures determined at room temperature and 109 K, respectively. The two pairs of points suggest that PRIN1 somehow depends on the temperature of the experiment. It is known (1) that temperature affects motion in the crystal, (2) that motion (more specifically: large amplitude libration) of a molecule leads to an apparent shortening of bonds, and (3) that the shortening becomes more pronounced as temperature increases.[43] This is what is observed: at room temperature the ligand distances are shorter (PRIN1 < 0) than at low temperature (PRIN1 > 0). Note that the effect is largest for the bonds C3C4 and C4C5 (Figure 3a) which are at the periphery of the $M(bpy)_3^{n+}$ complex where motion tends to be largest. This is illustrated in Figure 3b which shows average isotropic displacement parameters ($U_{eq}$ values) to be largest for atoms C3 and C4. Among the metal complexes for which $U_{eq}$'s are available in the published literature, the complex $[Ir(bpy)_3]^{3+}$ shows by far the largest $U_{eq}$ and the smallest value of PRIN1 (−0.038 Å). An analogous difference in thermal motion can be due to differences in molecular packing. This is documented in Figure 2 by, for example, the two points corresponding to $[Co(bpy)_3]^{2+}$ complexes. They have different crystal structures and different values of PRIN1 but similar values of PRIN2.

(43) Cruickshank, D. W. J. *Acta Crystallogr.* **1956**, *9*, 754.

**Table II.** Selected Values for Principal Component 1 (PRIN1)

| cation | anion | PRIN1 (295 K) | PRIN1 (110 K) | δ(PRIN1) (105–295 K) |
|---|---|---|---|---|
| bpy[20,19] | | −26.0 | 12.7 | 38.7 |
| $Hbpy^+$ [22,21] | $B_{10}H_{10}^{2-}$ | −16.3 | 15.8 | 32.1 |
| $Ru^{2+}$ [8] | 17.846 | −28.8 | 4.3 | 33.1 |
| $Hbpy^+$ | 19.915 | −54.1 | | |
| | $R\bar{3}c$ | −16.3 | | |
| | $I_2Br_3^-$ [24] | 15.6 | | |
| $Co^{2+}$ | $Cl^-$, $H_2O$, $C_2H_5OH$ [30] | −11.3 | | |
| | $Cl^-$, $tart^{2-}$ [37] | 19.0 | | |
| $H_2bpy^{2+}$ | $SO_3F^-$ [29] | −22.3 | | |
| | $B_{10}H_{10}^{2-}$ [22] | −3.6 | | |
| | $(SbCl_5)_4^{4-}$ [27] | 60.1 | | |

How do the $[Ni(bpy)_3]^{2+}$ complexes fit into this picture? They have all been measured at room temperature, and yet, they show very large values of PRIN1, corresponding, apparently, to very small motion of these complexes. This seems somewhat contradictory. However, all three structures have been refined without including hydrogen atoms in the model of electron density. It is common experience that this tends to increase bond distances between atoms carrying hydrogen atoms by hundredths of an Ångström. Suppressing hydrogen atoms affects the distances C2C3, C3C4, and C4C5 in particular, i.e., the same distances that are also susceptible to effects of thermal motion. The effects of neglecting hydrogens in the model of the $[Ni(bpy)_3]^{2+}$ are thus comparable to those found for the compounds with low molecular motion and lead to large values of PRIN1 (Figure 2).

These points are documented in some detail in Table II which shows a rather consistent difference of PRIN1 as a function of the difference in measurement temperature and a tendency for increasing PRIN1 with increasing bulk of the counterion. In summary, we conclude that PRIN1 is to be interpreted as reflecting those variations in bond distances which are due primarily to the temperature of the experiment, the model used to interpret the diffraction data, and possibly differences in molecular motion due to differences in packing.

## Results and Discussion

**A. Description of the Structures.** Selected interatomic distances and angles of III and α-II, together with the corresponding values of the room-temperature structure β-II, are given in Table III. Interatomic distances and angles of the three crystallographically independent complexes of α-II were averaged both within ($D_3$ symmetry) and between complexes. The table shows that the geometries of the Ru complexes are virtually indistinguishable in the three crystal structures. Figure 4 shows an illustration of the coordination geometry and the atomic labeling in III.

The three bpy ligands around the Ru atoms form a propeller-like trigonal arrangement in both structures. The coordination by the nitrogen atoms is close to octahedral, deviations consist of a compression of the coordination octahedron along the trigonal axis by ~0.5 Å and a trigonal twisting of ~10° away from ideal octahedral geometry.

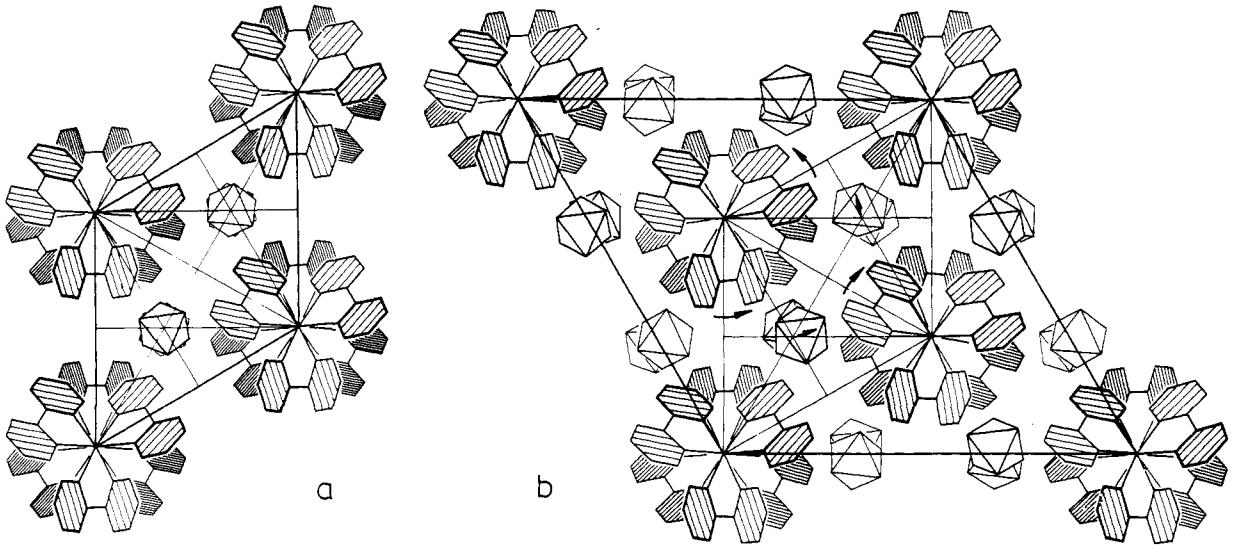


**Figure 5.** Comparison of the unit cells in the high (a) and low temperature (b) structure of $[Ru(bpy)_3](PF_6)_2$ (arrows in b show direction of displacements relative to the room temperature structure).

**$[Ru(bpy)_3](PF_6)_3$ (III).** $[Ru(bpy)_3](PF_6)_3$ is isostructural with $[Cr(bpy)_3](PF_6)_3$.[12] The six $[Ru(bpy)_3]^{3+}$ cations show site symmetry $D_3$. Cations of opposite chirality alternate along the 3-fold axis of the unit cell. The phosphorus atoms and the fluorine atoms F(3) and F(4) are located on 2-fold axes, whereas the remaining fluorine atoms are in general position. The $PF_6$ anions are of approximate octahedral symmetry, deviations from ideal angles being less than 0.5°: P–F bond distances vary between 1.582 and 1.600 Å.

**$[Ru(bpy)_3](PF_6)_2$ (II).** Overall, bond distances of the Ru complex cations in the $\alpha$-structure are slightly longer than in $\beta$-II as expected on the basis of the difference in temperature. Most of the relevant parameters lie within one standard deviation (Table III). The $PF_6$ anions are of approximately ideal octahedral geometry with P–F distances of 1.597 (11) Å at 105 K and 1.555 (21) Å at 298 K. The low temperature structure of $[Ru(bpy)_3](PF_6)_2$ ($\alpha$-II) is best described as a slight distortion of the packing in the room temperature structure ($\beta$-II). The relationship between the two unit cells is visualized in Figure 5. The packing in both phases is basically a hexagonal primitive arrangement of Ru atoms. The close packed layers are arranged perpendicular to [001] at $z \sim 1/4$ and $z \sim 3/4$. While the layers in $\beta$-II are exactly planar ($z = 1/4$), the Ru atoms in the $\alpha$-phase are located at slightly different heights (Ru(1): $z_1 = 0.2349$; Ru(2): $z_2 = 0.2484$; Ru(3): $z_3 = 0.2667$, the center of gravity is fixed at $z = 1/4$). The site symmetry of the complex ions is lowered from $D_3$ in $\beta$-II to $C_3$ in $\alpha$-II. $[Ru(bpy)_3]^{2+}$ ions of opposite chirality alternate along the 3-fold axes. The orientation of the Ru(1) complex cations (at $(0, 0, z_1)$) is practically unchanged with respect to $\beta$-II. It is rotated about the [001] axis by less than 1°. In contrast, the Ru(2) (at $^1/_3, ^2/_3, z_2$) and Ru(3) complexes (at $^2/_3, ^1/_3, z_3$) in $\alpha$-II are rotated relative to $\beta$-II by ~4° in a clockwise and anticlockwise direction, respectively.

In $\beta$-II the P atoms are located on positions of site symmetry 3 ($(0, ^1/_3, 0.37047)$; $(^1/_3, ^1/_3, 0.62953)$ with respect to the cell of $\alpha$-II); in the $\alpha$-form they are in general positions ((0.0195, 0.3560, 0.3659), (0.3097, 0.3271, 0.6342)). The shift with respect to the $\beta$-phase is marked by arrows in Figure 5. The overall shift in the $x$-$y$-plane is 0.39 Å for both P atoms. In the $z$ direction the difference of the P atom positions between both phases is less than 0.08 Å relative to the center of gravity of the Ru atoms. These displacements of the $PF_6$ octahedra are correlated with the rotations of the $Ru(bpy)_3$ as indicated in Figure 5b.

**B. Kinetic Aspects.** The electron self-exchange reaction

$$Ru(bpy)_3^{3+} + Ru'(bpy)_3^{2+} \xrightarrow{k} Ru(bpy)_3^{2+} + Ru'(bpy)_3^{3+}$$

proceeds with a rate constant $k = 4.2 \times 10^8$ $M^{-1}$ $s^{-1}$.[10,11] Within the framework of the Marcus–Hush approach the corresponding free energy of activation is conventionally expressed as a sum of several contributions, the Coulombic work term ($w_r$), the solvent reorganization energy ($\Delta G^*_{out}$), and the inner sphere activation energy ($\Delta G^*_{in}$).[44] $\Delta G^*_{in}$ depends primarily on the square of $\Delta r$,

**Table III.** Selected Interatomic Distances (Å) and Angles (deg) for III and II

| | | $[Ru(bpy)_3](PF_6)_2$ | |
|---|---|---|---|
| compound | $[Ru(bpy)_3](PF_6)_3$[a] | $\alpha$[b] | $\beta$ |
| temp, [K] | 105 | 105 | 298 |
| lattice const [Å] | | | |
| $a$ | 17.846 | 18.328 | 10.760 |
| $c$ | 19.915 | 16.216 | 16.391 |
| space group | $R\bar{3}c$ | $P31c$ | $P\bar{3}c1$ |
| $[Ru(bpy)_3]^{n+}$ | | | |
| $n$ | 3+ | 2+ | 2+ |
| site symmetry of Ru | 32 | 3 | 32 |
| distances, [Å] | | | |
| Ru–N | 2.057 (3) | 2.053 (2)[c] | 2.056 |
| C1–N | 1.360 (5) | 1.352 (2)[c] | 1.355 |
| C1–C2 | 1.389 (5) | 1.381 (3)[c] | 1.363 |
| C2–C3 | 1.381 (6) | 1.389 (3)[c] | 1.376 |
| C3–C4 | 1.389 (6) | 1.379 (3)[c] | 1.347 |
| C4–C5 | 1.379 (6) | 1.372 (3)[c] | 1.365 |
| C5–N | 1.353 (5) | 1.352 (2)[c] | 1.351 |
| C1–C1′ | 1.450 (7) | 1.482 (3)[c] | 1.476 |
| $h$[d] | 2.135 | 2.087 (30) | 2.097 |
| S[e] | 3.049 | 3.059 (24) | 3.062 |
| angles, [deg] | | | |
| N–C1–C1′–N′ | 11.0 | 6.6 (19) | 5.9 |
| trig twist | 50.9 | 51.3 (3) | 51.8 |
| C1–N–Ru | 115.0 (2) | 116.2 (3) | 115.9 |
| C5–N–Ru | 125.3 (3) | 125.5 (7) | 126.1 |
| C5–N–C1 | 119.4 (3) | 118.4 (7) | 117.9 |
| N–C1–C2 | 120.9 (3) | 121.9 (15) | 120.8 |
| C1–C2–C3 | 119.4 (4) | 119.0 (18) | 120.2 |
| C2–C3–C4 | 119.5 (4) | 119.0 (14) | 119.2 |
| C3–C4–C5 | 118.9 (4) | 119.4 (8) | 119.4 |
| C4–C5–N | 121.7 (4) | 122.2 (6) | 122.6 |
| N–Ru–N′[f] | 78.9 | 78.6 (2) | 78.6 |
| N–Ru–N′ | 90.4 | 89.4 (2) | 89.1 |
| N–Ru–N′ | 172.3 | 172.6 (2) | 173.0 |
| N–Ru–N′[g] | 95.6 | 95.7 (12) | 96.3 |
| $PF_6$ | | | |
| site symmetry of P | 2 | 1 | 3 |
| distances P–F | 1.591 (8) | 1.597 (11) | 1.54/1.57 |

[a] Esd's from structure factor least-squares calculation. [b] Averaged with respect to $D_3$ symmetry; esd's of mean. [c] Restrained structure factor least squares refinement (see text). [d] Height of the trigonal antiprism formed by N atoms of the bpy ligands. [e] Edge length of the basis of the trigonal antiprism. [f] Intraligand. [g] At base of trigonal antiprism.

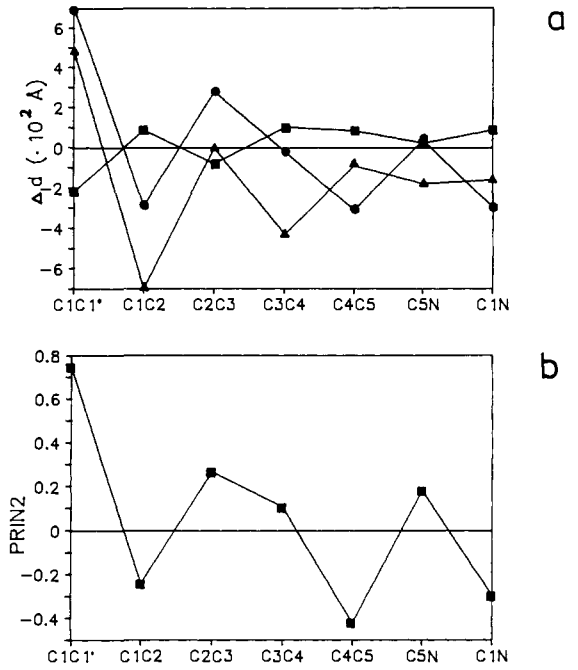


Figure 6. (a) Bond length differences $\Delta d(Ru^{3+}-Ru^{2+})$ (■), $\Delta d(Co^{2+}-Co^{+})$ (●), and $\Delta d(Ru^{2+}-{}^{*}Ru^{2+})$ (▲) and (b) coefficients of eigenvector PRIN2.

the difference of the metal-to-ligand distances in the two oxidation states. Our study shows the coordination geometries of $Ru(bpy)_3^{3+}$ and $Ru(bpy)_3^{2+}$ to be the same within experimental error. Thus $\Delta G^{*}_{in}$ does not contribute to the activation process for the $Ru(bpy)_3^{2+/3+}$ self-exchange. However, identical coordination geometries have also been demonstrated for the two encapsulated complexes $Ru(sar)^{3+}$ and $Ru(sar)^{2+}$ (sar = sarcophagine = 3,6,10,13,16,19-hexaazabicyclo[6.6.6]eicosane).[45,46] The self-exchange rate for this couple is $1.2 \times 10^5$ $M^{-1}$ $s^{-1}$, three orders of magnitude slower than for $Ru(bpy)_3^{2+/3+}$. To rationalize this shift in reactivity, two different contributions have to be considered: (i) $w_r$ and $\Delta G^{*}_{out}$: These depend only on the sizes of the reactants and on the distance between the metal centers in the activated complex. According to calculations within the classical limit[44] these two quantitites are only about 1.5 kcal $mol^{-1}$ larger for the sar complex than for the bipy complex (accounting for a difference in rate of a factor of $\sim 10$).[47] (ii) Acceleration of the electron transfer from the sar to the bpy complexes must therefore be attributed also to electronic effects.

**C. Aspects of Electronic Structure.** Szalda, Creutz, Mahajan, and Sutin[32] show for the $[Co(bpy)_3]^{2+/1+}$ couple and Mallick, Strommen, and Kincaid[48] for ground state $[Ru(bpy)_3]^{2+}$ and electronically excited $*[Ru(bpy)_3]^{2+}$ that the intraligand distances in bpy can be used as an indicator for aspects of the electronic structure of the complex cations. The pattern of differences in ligand distances is very similar between the pair $[Co(bpy)_3]^{2+/+}$ and the pair $[Ru(bpy)_3]^{2+}/*[Ru(bpy)_3]^{2+}$ (Figure 6a). The pattern is usually explained[32] in terms of backdonation of Co(I) into the $\pi^*$-LUMO of bpy or in terms of excitation of a $Ru(d\pi)$ electron into the same $\pi^*$-LUMO (Figure 7). From the nodal properties of $\pi^*$ it follows that population of this orbital clearly shortens the C1C1′ bond and possibly the C2C3 bond also, whereas

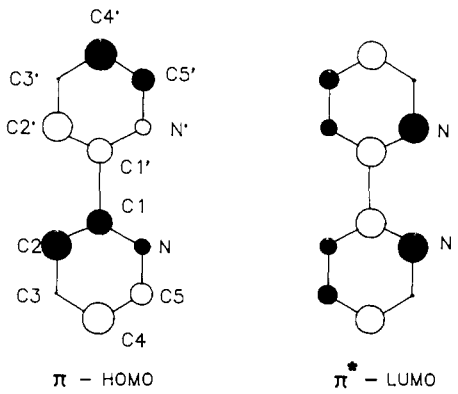


Figure 7. $\pi$ (HOMO) and $\pi^*$ (LUMO) orbital of the bpy ligand ($\alpha$(C) = 0, $\beta$(C–C) = $\beta$, $\alpha$(N) = 0.5$\beta$, $\beta$(C–N) = $\beta$) (radii of cycles proportional to the Hückel molecular orbital coefficients of the out-of-plane p orbitals: filled symbols represent positive phase of wave function).

the C1C2 and C3C4 bonds tend to be lengthened; this explanation is in general agreement with the patterns in Figure 6a.

The structure determinations of $[Ru(bpy)_3]^{3+}$ and $[Ru(bpy)_3]^{2+}$ provide a basis for an analogous comparison, especially because the temperatures of the measurement and the counter ions are the same for both structures (comparable PRIN1). According to the usual arguments based on $\pi$-backbonding ideas, Ru(II) is a better donor into $\pi^*$ than Ru(III). This is confirmed by comparing the Ru–N distances of the $[Ru(bpy)_3]^{n+}$ with those of the $[Ru(NH_3)_6]^{n+}$ complexes. For $n = 3$ the Ru–N distances in the bpy complex are only 0.049 Å shorter than in the $NH_3$ complex; for $n = 2$ the corresponding shortening is almost doubled, 0.089 Å. Along these lines C1C1′ is expected to be shorter for the Ru(II) complex than for the Ru(III) complex. The opposite is true! In fact, the entire pattern of differences in ligand distances (in Figure 6a) is reversed and seems to indicate that the Ru(III) complex shows better backdonation than the Ru(II) complex. Although comparisons of individual bond length differences in the $[Ru(bpy)_3]^{3+/2+}$ couple are hardly significant ($0.001\ (5) \le d \le 0.032\ (7)$ Å), the pattern of differences in the ligand distances is suggestive. The result is unexpected and contradicts the trend found in the Ru–N distances.

To put this result into a broader perspective, the data for all available $[M(bpy)_3]$ complexes of reasonable accuracy were compared through a principal component analysis (Experimental Section D). This analysis gives two main factors, one related to the temperature of measurement, to model and/or packing effects (discussed in the Experimenal Section) and, in second position of importance, a factor related to electronic structure (PRIN2).

**Principal Component 2.** The coefficients of the eigenvector PRIN2 (Figure 6b) imply—for positive PRIN2—lengthening of the bonds C1C1′, C2C3, C3C4, and C5N and shortening of the other intra-bpy bond lengths relative to their mean values. The main effect is found for the C1C1′ bond. The differences in distances implied by a positive difference in PRIN2 are very similar to the distance differences observed between $[Co(bpy)_3]^{2+}$ and $[Co(bpy)_3]^{1+}$ or between $[Ru(bpy)_3]^{2+}$ and $*[Ru(bpy)_3]^{2+}$ (Figure 6a). The similarity is taken as a strong indication that PRIN2 measures the changes in ligand distances due to electronic effects; an increase in PRIN2 between two related compounds would indicate a decrease in population of $\pi^*$, e.g., PRIN2 for $[Co(bpy)_3]^{+}$ with relatively strong backbonding is smaller than PRIN2 for $[Co(bpy)_3]^{2+}$ with relatively smaller backbonding. Analogously, PRIN2(*Ru(II)) = −0.036 Å is smaller than PRIN2(Ru(II)) = 0.014 Å. As far as the title compounds are concerned, it is found that PRIN2(Ru(III)) is smaller than PRIN2(Ru(II)), suggesting—as in the qualitative comparison above—that backbonding is better for Ru(III) than for Ru(II). This is in clear contradiction to what is found from a comparison of Ru–N distances in the respective bpy and $NH_3$ complexes.

It is tempting to resolve this contradiction by arguing that the hole in the $d_\pi^5$-shell of Ru(III) partially oxidizes the bpy ligand,

(44) Sutin, N. *Prog. Inorg. Chem.* **1983**, *30*, 441.
(45) Bernhard, P.; Sargeson, A. M. *Inorg. Chem.* **1987**, *26*, 4122.
(46) Bernhard, P.; Bürgi, H.-B.; Raselli, A.; Sargeson, A. M. *Inorg. Chem.* **1989**, *28*, 3234.
(47) The molecular van der Waals radii along and perpendicular to the 3-fold molecular symmetry axes are 5.0 and 3.3 Å for the [Ru sar] complexes, 4.8 and 4.4 Å for the $[Ru(bpy)_3]$ complexes with geometric means of 3.8 and 4.5 Å, respectively. The calculated rates at ionic strength 0.1 M are $10^6$ and $2 \times 10^7$.
(48) Mallick, P. K.; Strommen, D. P.; Kincaid, J. R. *J. Am. Chem. Soc.* **1990**, *112*, 1686.

thereby depopulating the ligand $\pi$-HOMO. Inspection of Figure 7 shows that the effect of depopulating $\pi$ is similar to that of populating $\pi^*$, at least as far as the bonds C1C1′ and C1C2 are concerned. Note, however, that *all* complexes with triple positive charge (except one) are found in a field which does not overlap with the field of M(II) complexes and is intermediate between the field of M(II) complexes and the point representing the Co(I) complex (Figure 2). In the field of complexes with triple positive charge both $d_\pi^5$ and $d_\pi^6$ electronic configurations are found. This shows that $\pi \rightarrow d_\pi$ is an unlikely explanation for the observed structural patterns and indicates that charge may have a more important influence on the geometry of bpy in its metal complexes than partial ligand oxidation by an incomplete $d_\pi$-subshell. Note, that the only exception to the grouping by charge is the Cr(III) complex with three holes in its electronic configuration. The bpy and protonated bpy structures are distributed throughout the M(II) and M(III) complexes.

In summary, we feel that the usual backbonding model does not provide a consistent explanation of the relationships between charge, M–N distances, bpy geometry, and electronic structure in $[M(bpy)_3]^{n+}$ complexes. In part this may be due to the limited accuracy of the available data. The crystal structure analyses of $[Ni(bpy)_3]^{2+}$ have already been mentioned as an example of systematic error in the bond distances due to omission of hydrogen atoms from the model. The structure of $[Ir(bpy)_3]^{3+}$ is judged unreliable because it shows large displacement parameters and some unusual CCC and CCN bond angles. Further clarification of the relationship between electronic and geometric structure in $[M(bpy)_3]^{n+}$ complexes will therefore have to rely on a combination of improved structural data and more sophisticated theoretical investigations. However, there is little doubt in our minds, that the inconsistency mentioned above is real. It became apparent with the help of quantitative principal component analysis, which at present would seem the most reliable procedure to distinguish as well as is possible the electronic effects of interest from effects related to data collection and data treatment. At present, we are unable to give a consistent description of electronic effects on the M–N, N–C, and C–C distances in $M(bpy)_3^{n+}$ complexes. To the best of our knowledge the inconsistency has not been noted before.

**Acknowledgment.** We gratefully acknowledge financial help by the "Schweizerischer Nationalfonds zur Förderung der wissenschaftlichen Forschung", Grant Nos. 20-5370.87, 20-29585.90, and 20-26448.89. We thank Johnson Matthey for a loan of $RuCl_3 \cdot xH_2O$ and CIBA-GEIGY for the microanalyses.

**Supplementary Material Available:** Listings of crystal data, intensity collection and refinement parameters, atomic positional parameters, calculated hydrogen positional parameters, and anisotropic displacement parameters (7 pages); listing of observed and calculated structure factors (12 pages). Ordering information is given on any current masthead page.

# 1,2-Disiladioxetanes: Structure, Rearrangement, and Reactivity

**Kirsten L. McKillop, Gregory R. Gillette, Douglas R. Powell, and Robert West***

*Contribution from the Department of Chemistry, University of Wisconsin, Madison, Wisconsin 53706.* *Received December 2, 1991*

**Abstract:** The low-temperature reaction of (*E*)-1,2-dimesityl-1,2-di-*tert*-butyldisilene (**1a**) with dioxygen gives (*E*)-1,2-dimesityl-1,2-di-*tert*-butyldisiladioxetane (**2a**), the structure of which has been established by X-ray crystallographic analysis. This result establishes that both oxidation of **1a** and rearrangement of **2a** to 1,3-cyclodisiloxane **4a** take place with retention of configuration at silicon. Disiladioxetane **2a** forms monoclinic crystals, space group *C*2/*c*. Extra electron density found above and below the Si–Si bond was shown by $^1H$ and solid-state $^{29}Si$ NMR to be due to **4a**, arising from rearrangement of **2a** in the solid. X-ray crystal structures were determined for crystals that were 5.6%, 15.2%, and 20.3% rearranged. Cell dimensions for the 5.6% rearranged crystal are $a$ = 12.549 (7) Å, $b$ = 12.174 (7) Å, $c$ = 17.133 (7) Å, $b$ = 103.94 (4)°, $V$ = 2529 (2) Å$^3$ ($Z$ = 4). The rearrangement of **2a** in solution is first order with $E_a$ = +21.7 ± 1.0 kcal mol$^{-1}$, $\Delta H^\ddagger$ = 21.1 ± 1.4 kcal mol$^{-1}$, and $\Delta S^\ddagger$ = −9.0 ± 4.5 cal K$^{-1}$ mol$^{-1}$. Isotope labeling studies with $^{18}O$ showed the rearrangement to be intramolecular in the solid and in solution. In the presence of phosphines or sulfides, **2a** is partially deoxygenated to form disilaoxirane **3a**.

## Introduction

Although alkenes react rapidly with singlet dioxygen,[1] reaction with triplet dioxygen is normally slow. Exceptions are very electron-rich alkenes such as tetraaminoethylenes,[2] alkenes with low-lying triplet states such as cyclobutadienes,[3] and ketenes.[4] For other alkenes, $^3O_2$ oxidation takes place only catalytically or at high temperatures.

**Scheme I.** Oxidation of Disilenes with $^3O_2$

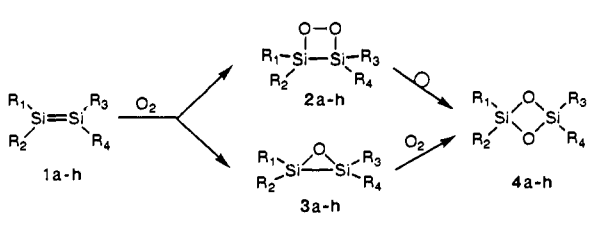


Disilenes have much lower oxidation potentials than olefins,[5] and they are correspondingly much more reactive toward $^3O_2$. The

(1) See: Bartlett, P. D.; Landis, M. E., Chapter 7; Schaap, A. P.; Zaklika, K. A., Chapter 6. In *Singlet Oxygen*; Wasserman, H. H., Murray, R. W., Eds.; Academic Press: New York, 1979.
(2) Urry, W. H.; Sheeto, J. *Photochem. Photobiol.* **1965**, *4*, 1067.
(3) Meijer, E. W.; Wynberg, H. *Tetrahedron Lett.* **1981**, *22*, 785. Maier, G. *Angew. Chem., Int. Ed. Engl.* **1974**, *13*, 425.
(4) Turro, N. J.; Chow, M.-F.; Ito, Y. *J. Am. Chem. Soc.* **1978**, *100*, 5880.

0002-7863/92/1514-5203$03.00/0 